2023-24-0174 Published 28 Aug 2023

Initial Development of a Physics-Aware Machine Learning Framework for Soot Mass Prediction in Gasoline Direct Injection Engines

Bharat Jayaprakash, Brady Wilmer, and William F. Northrop University of Minnesota-Twin Cities

Citation: Jayaprakash, B., Wilmer, B., and Northrop, W.F., "Initial Development of a Physics-Aware Machine Learning Framework for Soot Mass Prediction in Gasoline Direct Injection Engines," SAE Technical Paper 2023-24-0174, 2023, doi:10.4271/2023-24-0174.

Received: 28 May 2023 Revised: 30 Jun 2023 Accepted: 30 Jun 2023

Abstract

Calibration of automotive engines to ensure compliance with emission regulations is a critical phase in product development. Control of engine-out particulate emissions, which directly impact the environment and public health, is particularly important. Detailed physics-based models are typically used to gain a rich understanding of the complex physical phenomena that drive the soot particle formation in an engine cylinder. However, such models often fail to correctly represent the highly dynamic nature of the underlying mechanisms under transient combustion conditions. Moreover, most physics-based models were initially developed for diesel engine applications and their applicability to gasoline engines remains questionable due to differences in flame structure and fuel-wall interactions. Black-box models have been previously proposed to predict engine-out soot emissions, but their lack of physical interpretability is an unsolved drawback. To address these limitations, we present a physics-aware twin-model machine learning framework to predict and analyze engine-out soot mass from a gasoline direct injection (GDI) engine. The framework combines a physics-based model with a bagging-type ensemble learning model that both maintains high accuracy and allows physical interpretation of results without using computationally intensive high-fidelity models. This work shows why a one-model-fits-all approach fails in the case of predicting soot emissions due to clustered co-occurrences of operating conditions that cause non-compliant behavior. We compare the performance of the proposed framework with that of the standalone baseline model and a feed-forward deep neural network. Using WLTP data from a 2.0L naturally aspirated GDI engine, the proposed framework predicts engine-out soot mass with an improvement of 29% in the R^2 value and 21% in the root mean squared error from the baseline physics-based model, without compromising physical interpretability. These improvements are significant enough to warrant further framework development with additional engine datasets.

Introduction

Air pollution caused by conventional IC-engine-powered vehicles is a major concern globally, with general scientific consensus confirming its impact on the environment and public health. In 2019, an estimated 86% of urban inhabitants lived in conditions that exceeded WHO's 2005 guideline annual average $PM_{2.5}$ concentration (10 $\mu g/m3$), resulting in an excess of 1.8 million deaths [1]. In the same study, the average population-weighted $PM_{2.5}$ concentration across all urban areas globally was 35 $\mu g/m3$ – equivalent to seven times the revised 2021 WHO guideline for annual average $PM_{2.5}$ concentration (5 $\mu g/m3$). The Joint Research Centre (JRC) of the European Commission quantified road transportation's average contribution to $PM_{2.5}$ emissions in 150 urban areas at 14%, rising to 39% in the larger urban cities [2]. A 2017 study [3] expanded known toxicological mechanisms in humans caused by soot that lead to cancer, respiratory diseases, and cardiovascular dysfunctions. A 2012 WHO report [4] concluded that a reduction in exposure to $PM_{2.5}$ and other combustion products leads to a reduction in the health effects associated with PM. Compared to port fuel-injected (PFI) engines, GDI engines have been reported to emit exhaust gases with higher concentrations of PM [5] due to incomplete fuel vaporization and gas-phase mixing [6]. Furthermore, GDI engines without filtration produce even higher concentrations of ultrafine particles compared to diesel engines fitted with diesel particle filters (DPF) [7].

It is known that direct gasoline fuel injection can result in incomplete fuel evaporation and subsequent piston and wall wetting. This creates fuel-rich hotspots that undergo nucleation, growth, and oxidation under high-temperature conditions, ultimately forming particulate matter. Although the chemical kinetics of soot generation are highly complex and not fully understood, it is generally agreed upon by researchers that gaseous polycyclic aromatic hydrocarbons (PAHs) are highly influential in soot formation. In the absence of significant concentrations of aromatics in the fuel, the synthesis and growth of PAHs, and subsequently the

production of soot, would be constrained by the aromatic ring growth that results from reactions involving aliphatic chemicals [8].

Strict particulate matter regulations for gasoline engines have accelerated the development of portable emission measuring instrumentation and the integration of gasoline particulate filters (GPFs) into the vehicle's exhaust system. GPFs are used in modern gasoline engines to control the release of ultrafine particles from the tailpipe. They are typically made of synthetic ceramic, have a honeycomb structure, and may either be a separate unit or integrated with the vehicle's three-way-catalyst [9]. To complement these control and measurement devices, modeling and predicting particulate emissions is of keen interest to researchers and manufacturers alike. Accurately modeling soot emissions provides insights into the underlying mechanisms and helps develop design strategies to reduce particulate emissions.

Soot models from the current literature can be classified into three categories: empirical, semi-empirical, and detailed theoretical [10]. Empirical soot models ([11, 12]) generally consider the competing reactions of soot formation and soot oxidation. Their implementations are computationally intensive and are typically accomplished within high-fidelity CFD software codes. Semi-empirical soot models ([13, 14, 15]) aim to reduce the computational cost by simplifying the kinetic equations of soot formation and oxidation using valid approximations. However, empirical and semi-empirical models have multiple drawbacks which include the fact that they do not consider the effects of particle growth and the physical interactions of soot particles. De-tailed theoretical models ([16]) combine gas-phase kinetic equations with phenomenological soot models to form high-dimensional frameworks for modeling soot emissions. The high dimensionality and computational costs of such models make them poor candidates for modeling spatiotemporal emissions at engine-relevant timescales.

Using data-driven methods for predicting emissions has become increasingly popular due to the availability of high-quality data, advancements in machine learning models, and accessibility of more powerful computational resources. Laboratory engine testing and instrumented vehicles driven under real-world conditions are extremely reliable sources of high-quality data. Deep feed-forward neural networks and support vector machines (SVMs) are black-box data-driven models prominently used for emissions prediction. Such models have sufficient capability to numerically imitate underlying mechanisms from the training data. However, they are incapable of accurately responding to changes in the underlying mechanisms, have unreliable extrapolation capacity for operating conditions outside of the training data, and completely lack physical interpretability. Grey-box models combine interpretable physics-based theoretical structures and opaque data-driven methods. Such models have been used for predicting NO_x, CO and HC emissions ([17, 18]). Implementation of grey-box models for modeling soot emissions has thus far been limited to compression ignition engines [19]. Differences in flame structure and fuel-wall interactions between compression ignition engines and spark ignition engines limit the applicability of such models.

This study aims to address the limitations of current grey-box models with the development of a physics-aware twin-model machine-learning framework to predict and analyze engine-out soot mass from a GDI engine. The framework comprises a physics-based model and a random forest regression model. This combination maintains high prediction accuracy and allows physical interpretation of results. The study highlights the inadequacy of one-model-fits-all approaches in predicting soot emissions due to the occurrence of clustered non-compliant behavior caused by various operating conditions. The proposed framework's performance is compared with a standalone baseline model, a feed-forward deep neural network, and a recurrent neural network.

Methodology

Laboratory Dataset and Test Setup

The dataset used in this study contains 1 Hz time resolution data from a BMW N32B20 naturally aspirated 2.0 L in-line four-cylinder gasoline direct injection (GDI) engine. Some of the data were used in a previous study by Bock et al. [20]. The engine is equipped with a National Instruments Powertrain Controls engine controller to allow full control of the engine. Basic engine specifications are shown in Table 1.

The engine was coupled to an engine dynamometer and used a virtual drivetrain model to simulate the drivetrain components found in a production vehicle and forces experience by a vehicle on road. This model has been thoroughly described in previous work [20]. The virtual drivetrain model uses driveline force, drag, rolling resistance, and braking force to determine the net force on the modeled vehicle and the corresponding acceleration. Acceleration at each time interval was used to update modeled vehicle road speed and control engine conditions to match on-road behavior. Bock et al. performed WLTP drive cycle testing using this engine coupled with the virtual drivetrain model, specifically looking at the first 200 seconds when the PM emissions are higher due to cold start conditions. The influence of fuel properties was examined by testing six different fuels with varying ethanol concentrations, aromatics concentrations, and volatility [20]. Three replicate drive cycles with each fuel were conducted to

TABLE 1 Parameters of Engine Used to Generate Dataset

Engine Model Number	N32B20
Displacement	1995 cc
Bore	84 mm
Stroke	90 mm
Compression Ratio	12:1
Rated Power	125 kW (6700 rpm)
Rated Torque	210 Nm (4250 rpm)
Induction	Naturally Aspirated
Injection	Central Spray Guided Piezo Injectors
Max Rail Pressure	200 bar

generate this dataset with a total of 3618 data vectors. Engine-out soot mass was measured with an AVL photo-acoustic Microsoot Sensor (MSS).

Physics-based Soot Mass Model

A widely used empirical engine-out soot mass model applicable for engine simulations was proposed by Hiroyasu et al. [11]. The model employs two equations, one for the rate of formation of soot and the other for the rate of oxidation of soot.

$$\frac{dm_s}{dt} = \frac{dm_s f}{dt} - \frac{dm_{sc}}{dt} \tag{1}$$

$$\frac{dm_{sf}}{dt} A_f * m_{fg} * p^{0.5} * exp\left(-\frac{E_f}{RT}\right) \tag{2}$$

$$\frac{dm_{sc}}{dt} = A_c * m_s * X_{O_2} * p^{1.8} * exp\left(-\frac{E_{sc}}{RT}\right) \tag{3}$$

where, m_s is the mass of net soot, m_{sf} is the mass of formed soot, m_{sc} is the mass of oxidized soot, m_{fg} is the mass of vaporized fuel, p is the cylinder pressure, X_{O_2} is the mole fraction of oxygen during combustion, T is the cylinder temperature, E_f and E_{sc} are the activation energies of soot formation and soot oxidation, A_f and A_c are constants.

Inspired by the model proposed by Hiroyasu et al., a simplified physics-based soot mass model that can be used for high-frequency discrete-time data is presented. The model equation to calculate the instantaneous engine-out soot mass is given by Equation 4.

$$\begin{aligned} m_{s_k} &= a * m_{fg} * p^{0.5} * exp\left(-\frac{-b}{T_{adiab}}\right) \\ &+ \left(q - c * m_{O_2} * p^{1.8} * exp\left(\frac{-d}{T_{adiab}}\right)\right) * m_{s_{k-1}} \end{aligned} \tag{4}$$

where m_{s_k} is the instantaneous engine-out soot mass at time k, m_{fg} is the mass of injected fuel, p is the cylinder pressure, m_{O_2} is the mass of oxygen available during combustion, T_{adiab} is the adiabatic flame temperature during combustion, and a, b, c, d, and q are tunable coefficients.

Calculating Adiabatic Flame Temperature

The adiabatic flame temperature is defined as the temperature of the combustion products in the combustion chamber under the assumption that the inter-species reactions are adiabatic in nature, i.e. all the heat produced during the reactions is completely used to increase the temperature of the product species. Although the adiabatic flame temperature is not the exact temperature at which soot forms during combustion, the relative change in adiabatic flame temperature between engine conditions is a significant factor in soot formation and oxidation. The underlying assumption for using the adiabatic flame temperature in Equation 4 is that the tunable coefficients a, b, c and d collectively act as appropriate correction factors. The energy balance equation used to calculate the adiabatic flame temperature is:

$$LHV * MW_{fuel} = \sum_{i=CO_2,H_2O,N_2,O_2} n_i * \int_{T_c}^{T_{adiab}} c_{p,i} dT \tag{5}$$

where LHV is the lower heating value of gasoline fuel, MW_{fuel} is the molecular weight of gasoline in kg/mol, n_i is the number of moles of species i per engine cycle where $i \in \{CO_2, H_2O, N_2, O_2\}$, c_{pi} is the temperature-dependent specific heat values of species i in $J/K/mol$, T_c is the combustion chamber temperature at the end of the compression stroke, and T_{adiab} is the adiabatic flame temperature in K. The temperature-dependent equations for $c_{p,i}$ are obtained from the lookup tables in [21].

Calculating Remaining Variables

The mass of injected fuel, m_{fg}, was measured by a Coriolis flow meter which measured the total fuel flow rate delivered to the engine. The cylinder pressure, p, is approximated to be equal to the brake mean effective pressure (*BMEP bar*). It is important to note that the BMEP is not an exact estimate of the instantaneous cylinder pressure during soot formation, but does provide a measure of changing engine load. The mass of oxygen available during combustion, m_{O2}, is determined from the total flow rate of intake air which is measured by a laminar flow element. The ground truth values of measured engine-out soot (*Soot*) are obtained from the laboratory dataset.

Soot Mass Prediction Using Baseline Model

An effective way to determine the appropriate values of the coefficients in Equation 4 to obtain an accurate fit is to use non-linear regression. The SciPy python package [22] provides a non-linear regression function (*curve_fit*) that uses the Levenberg-Marquardt algorithm, also known as the damped least-squares (DLS) method to determine the regression coefficients. Without enforcing boundary conditions, and setting the maximum number of function evaluations to 500,000, the values of the obtained regression coefficients and the performance metrics are shown in Table 2. The performance metrics used for assessing the predictions are the root mean squared error (RMSE), the mean absolute error (MAE), and the coefficient of determination (R^2). The predicted soot mass using the regressed model is plotted against the ground truth in Figure 1. Additionally, the predicted and measured cumulative engine-out soot mass are plotted in Figure 2.

Considering an error range of $\pm 5 mg/m^3$, the proposed physics-based model occasionally produces inaccurate predictions. The model is more likely to underestimate the value of the target variable than to overestimate it, and the errors in the underestimations are typically larger than those in the

TABLE 2 Regression Coefficients and Performance Metrics of Baseline model

Metric/Parameter	Value
a	0.164
b	-4.938e+03
c	2.452e-06
d	-1.154e+04
q	6.955e-01
RMSE	2.691
MAE	1.287
R^2	0.594

FIGURE 1 Engine-out soot mass prediction using the proposed physics-based model

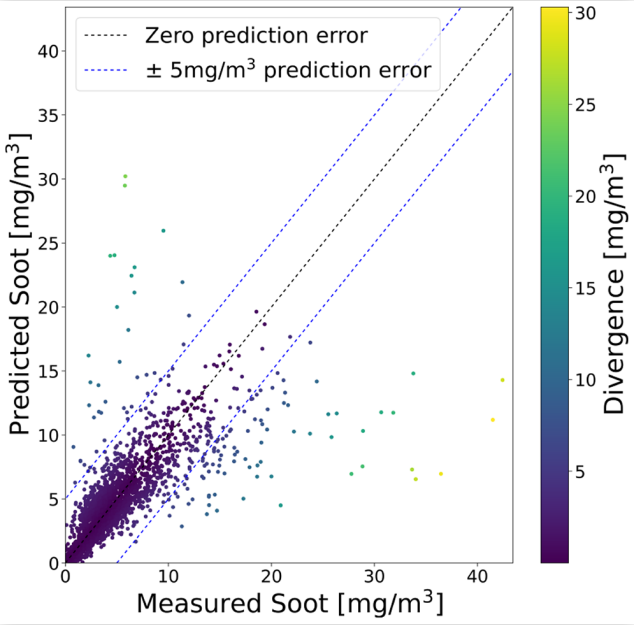

FIGURE 2 Engine-out cumulative soot mass using the proposed physics-based model

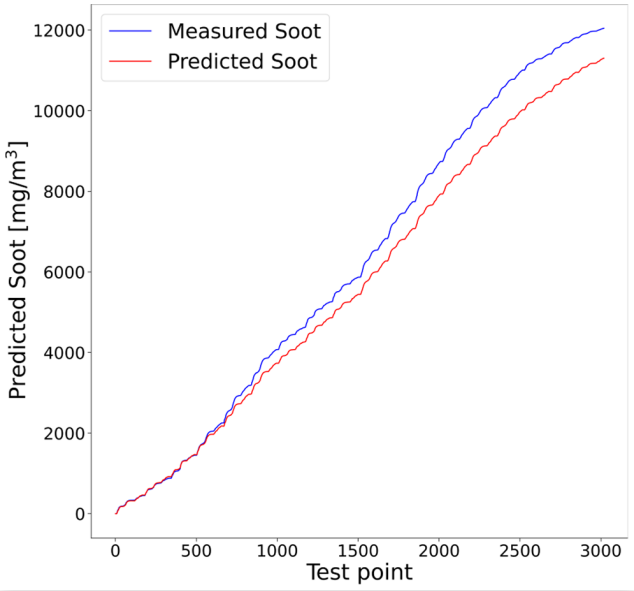

overestimations. The observation of prediction outliers called for a deeper investigation into their nature and the engine operating conditions that led to them.

Divergent Window Co-occurrence Patterns

Predicted data points are classified as outliers in Figure 1 based on their position relative to the $\pm 5 mg/m^3$ error lines. To investigate whether the outliers are a result of anomalous patterns, a Divergent Window Co-occurrence (DWC) Pattern Detection algorithm is deployed. This algorithm applies the methods developed by Ali et al. [23] to the engine-out emissions domain. It takes in a set of features and constraints as inputs and outputs all statistically significant DWC patterns. A divergent window of soot emissions refers to a period of L seconds in a time series of input features within which the mean of the prediction errors (absolute difference between predicted and observed soot mass value) of the baseline approach exceed an input divergence threshold (*meanThreshold*). A co-occurrence pattern in a time series of input features is similar to a sequential association pattern except for the use of a spatial statistical interest measure, i.e., Ripley's Cross-K function (K_r) specialized for time series data. In essence, the DWC pattern represents a set of input attributes and their respective value ranges that tend to occur concurrently across multiple divergent time windows and have Cross-K function values above a given threshold (K_{rlower}) and support (i.e., the number of divergent windows in a pattern divided by the total number of time windows) greater than a pre-defined value (*supportThreshold*). The DWC pattern detection algorithm was deployed on 3 parameter sets as shown in Table 3.

Set 1 contained 6 parameters taken directly from the laboratory test dataset that can characterize different driving patterns and could potentially influence the production of soot. Set 2 contained 4 parameters that are the approximate time derivatives of the parameters contained in Set 1. This set was constructed with the aim of getting a better understanding of the effect of transient operating conditions on emitted soot. Set 3 contained the 4 parameters that were used in the physics-based model. The aim of this set was to check whether the patterns obtained from Set 1 and Set 2 could be translated into patterns in the input features of the physics-based model. The Cross-K function lower bound threshold K_{rlower} was set to 2, the *supportThreshold* value to 0.004, the *meanThreshold* to $5 mg/m^3$, the window length *L* to 3 seconds, and the lag to 2 seconds.

The top five most significant patterns mined using Parameter Set 1 and Set 2 are listed in Table 4. It contains the parameters that co-occur in each pattern and are listed in the

TABLE 3 Parameter Sets for DWC Pattern Detection

Parameter Set	Parameters Present
Set 1	*engSpd, fuelRate, intakeT, intakeP, brakeTorque, airRate*
Set 2	*engSpdDelta, fuelRateDelta, brakeTorqueDelta, airRateDelta*
Set 3	m_{O2}, p, T_{adiab}, m_{fg}

TABLE 4 Description of the top four most statistically significant DWC patterns using parameter Set1 and Set2

Pattern	Co-occurrence	Cross-K	Confidence
Pattern1	*engSpd*: $\{S_2\ S_2\ S_3\}$ *intakeP:* $\{P_5\ P_6\ P_5\}$ *airRate:* $\{A_3\ A_3\ A_3\}$	67.65	1.0
Pattern2	*engSpd*: $\{S_2\ S_2\ S_2\}$ *fuelRate:* $\{F_1\ F_2\ F_4\}$ *intakeT:* $\{T_3\ T_3\ T_3\}$	60.71	1.0
Pattern3	*engSpdDelta*: $\{Sd_5\ Sd_5\ Sd_5\}$ *brakeT orqueDelta:* $\{Bd_5\ Bd_6\ Bd_5\}$ *airRateDelta:* $\{Ad_5\ Ad_5\ Ad_4\}$	52.04	0.86
Pattern4	*engSpdDelta*: $\{Sd_5\ Sd_5\ Sd_5\}$ *fuelRateDelta:* $\{Fd_4\ Fd_5\ Fd_6\}$	49.67	0.82
Pattern5	*brakeTorque:* $\{B_6\ B_6\ B_7\}$ *airRate:* $\{A_3\ A_3\ A_4\}$	37.60	0.78

decreasing order of their statistical significance (represented by the Cross-K values). The confidence measure is used to assess the statistical nature of the co-occurrence pattern. It determines the fraction of pattern instances in the dataset that co-occurs with a divergent window instance. A confidence value of 1.0 for pattern 'A' indicates that all instances of pattern 'A' co-occur with a divergent window instance. Each of the parameters is uniformly discretized into 10 bins. The letter representations S, P, Sd, etc. along with the subscripts indicate the magnitude of the attributes in a DWC pattern. For e.g., in the dataset, *engSpd* spans from around 800 rpm to around 2500 rpm. Considering the 10-bin discretization, S_2, as seen in *Pattern*1 of Table 4, points to the second bin of the discretized parameter *engSpd*, which covers the range of 970 rpm to 1140 rpm. It can be observed that the significant patterns mentioned in the table belong to different representations of the transient operating conditions of the engine. Transient parameters that lead to divergent patterns include changing engine speed, torque, and air flow rate.

The significant patterns mined using Parameter Set 3 are listed in Table 5. It can be observed that these patterns have lower Cross-K and confidence values relative to the patterns mined using the earlier parameter sets. However, the existence of these patterns supports the assumption that the detected outliers can be represented using a finite set of co-occurring feature patterns. This confirms that a 'one-model-fits-all' approach fails in the case of predicting soot emissions.

TABLE 5 Description of the top four most statistically significant DWC patterns using parameter Set3

Pattern	Co-occurrence	Cross-K	Confidence
Pattern1	m_{O_2}: $\{O_0\ O_0\ O_1\}$ *p:* $\{P_1\ P_2\ P_3\}$ T_{adiab}: $\{T_1\ T_1\ T_2\}$ m_{fg}: $\{F_0\ F_1\ F_2\}$	42.51	0.72
Pattern2	m_{O_2}: $\{O_1\ O_2\ O_0\}$	40.15	0.78
Pattern3	m_{fg}: $\{F_1\ F_1\ F_3\}$	30.70	0.67
Pattern4	m_{O_2}: $\{O_1\ O_1\ O_1\}$ *p:* $\{P_3\ P_3\ P_4\}$	29.10	0.73

Outlier Classification Tree

The DWC pattern detection algorithm was successful in mining the statistically significant co-occurrence patterns from the input features of the physics-based model. However, the relatively lower confidence measure values of the mined patterns called for the implementation of an alternative methodology for detecting outliers. A decision-tree-based Outlier Classification Tree (OCT) is presented as an alternative. Decision trees are binary trees (each parent node splits into two children nodes) which help predict a target value or class using feature variables. A decision tree classifier model is chosen for multiple reasons. First, decision trees predict target variables by learning simple decision rules inferred from the input data. Such models can be trained to learn the decisions based on the input feature patterns in the outliers. Second, decision trees are white box models. The inference for a classification instance can be easily explained by Boolean Logic. Third, deep-enough decision trees have high accuracy in supervised classification tasks.

The Outlier Classification Problem is defined as:

- **Input:** Set of input engine features S at time t
- **Output:** Binary classification label (0: Inlier, 1: Outlier) for input instance S and outlier classification criterion C_o
- **Objective:** Classification accuracy on new instance S_{new}
- **Constraints:** Maximum tree depth, the minimum sample size for splitting nodes

The outlier classification criterion C_o is the condition used for ground-truth classification of an instance S, and is represented by:

$$C_o = \begin{cases} 1, & \text{if } \left| y(S) - \check{y}(S) \right| > 5mg/m^3 \\ 0, & \text{else} \end{cases} \tag{6}$$

where $y(S)$ is the observed engine-out soot mass for input instance S and $\hat{y}(S)$ is the predicted engine-out soot mass for input instance S using the physics-based model.

The first version of the OCT was trained using an extended set of input features from the physics-based model, which included certain attributes that contributed to statistically significant DWC patterns. The complete list of input features is given in Table 6. The first task for designing the

TABLE 6 Initial input features for Outlier Classification Tree

Feature	Feature Symbol
m_{O_2}	X1
p	X2
T_{adiab}	X3
m_{fg}	X4
$m_{s_{k-1}}$	X5
engSpd	X6
brakeT orque	X7
engSpdDelta	X8
brakeT orqueDelta	X9
fuelRateDelta	X10

OCT was to determine the appropriate set of input features from the exhaustive list in Table 6. Feature elimination was done by comparing the feature importance (FI) measures of each input feature. The tree was trained on the original dataset with an 80%-20% train-test split for 20 iterations. The maximum tree depth was set to 6. The FI values and classification accuracy were recorded for each iteration. Figure 3 illustrates the mean FI values with their respective error bars. Feature *X*5 (engine-out soot mass with a 1-time-step lag) had the highest FI values and features *X*2, *X*7, and *X*8 had the lowest FI values. Based on the relative FI values, the extended list of input features was narrowed down to the 6 features that had the highest FI values. They are listed in Table 7.

The OCT was then further trained on different values of the maximum tree depth constraint. The mean accuracy values were recorded for each value of tree depth and the trend is shown in Figure 4. The scatter plots in Figure 5 illustrate the outlier classification performance of the OCT. The input features of the points plotted in Figure 5a are fed into the OCT as input and the outlier points plotted in Figure 5b is the produced as output. A sample model of the OCT with a tree depth of 4 is illustrated in Figure 15 in the Appendix section.

FIGURE 3 Error Box plot of feature importance for OCT

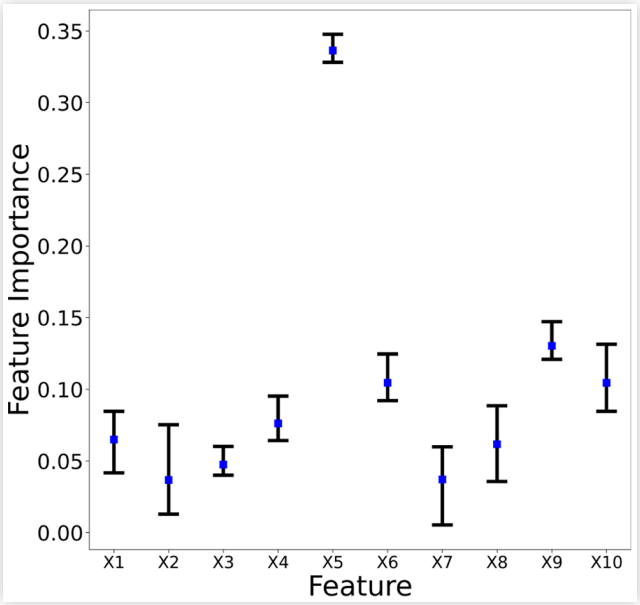

TABLE 7 Final input features for the OCT

Feature	Feature Symbol
m_{O_2}	X1
m_{fg}	X4
m_{sk-1}	X5
engSpd	X6
brakeT orqueDelta	X9
fuelRateDelta	X10

FIGURE 4 Classification accuracy trend on test dataset with varying tree depth

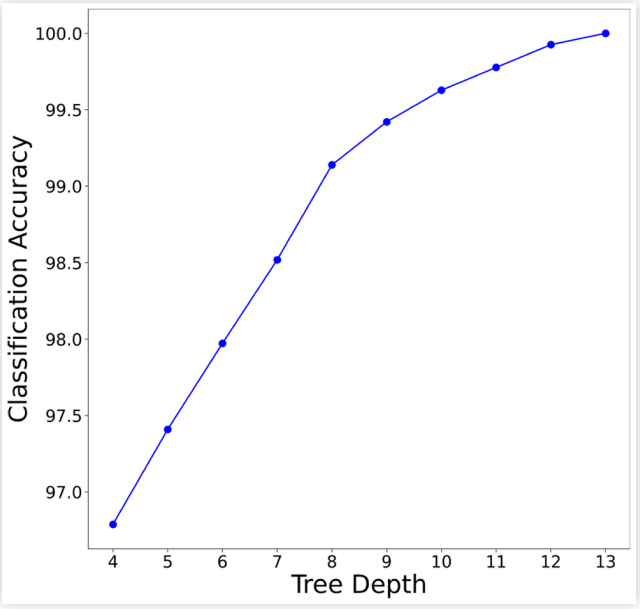

Physics-based Ensemble Learning Model

The physics-based model cannot accurately predict engine-out soot mass from the input data points classified as outliers by the OCT. A physics-based random forest regressor model is presented to predict soot mass for the outlier points only. A Random forest regressor (RFR) [24] is a type of ensemble learning model that consists of a set of decision trees (also known as regression trees). Ensemble learning models like the RFR involve using an ensemble of low-strength machine learning models in place of a single, high-strength model to obtain accurate predictions in highly heterogenous datasets. RFR models have previously shown better predictive accuracies than other ensemble models such as XGBoost and Gradient Boost for predicting vehicle emissions using real-world driving datasets [18]. While the combination of decision tree models makes the interpretation of the overall ensemble more complex than each of its compounding tree learners, RFR model inferences can be explained to a certain extent by using post-hoc explainability techniques like feature relevance analysis [25].

The initial feature set used for the RFR model is the same as that used for the OCT as shown in Table 6. It includes the parameters from the physics-based model and some measurable engine parameters from the laboratory test dataset. Parameters that can be tuned for the RFR model are the number of decision trees (*nEstimators*), the threshold for the maximum depth of individual trees (*maxDepth*), and the minimum number of samples in a node that cannot be further divided (*minSampleSplit*). A default set of values for the tunable parameters (*nEstimators* = 20, *maxDepth* = 10, *minSampleSplit* = 3) was chosen for the initial training run. The ground truth values of the engine-out soot mass were taken directly from the laboratory test dataset. The tree

FIGURE 5 Comparison of outlier and inlier points of the baseline model with those classified by the OCT

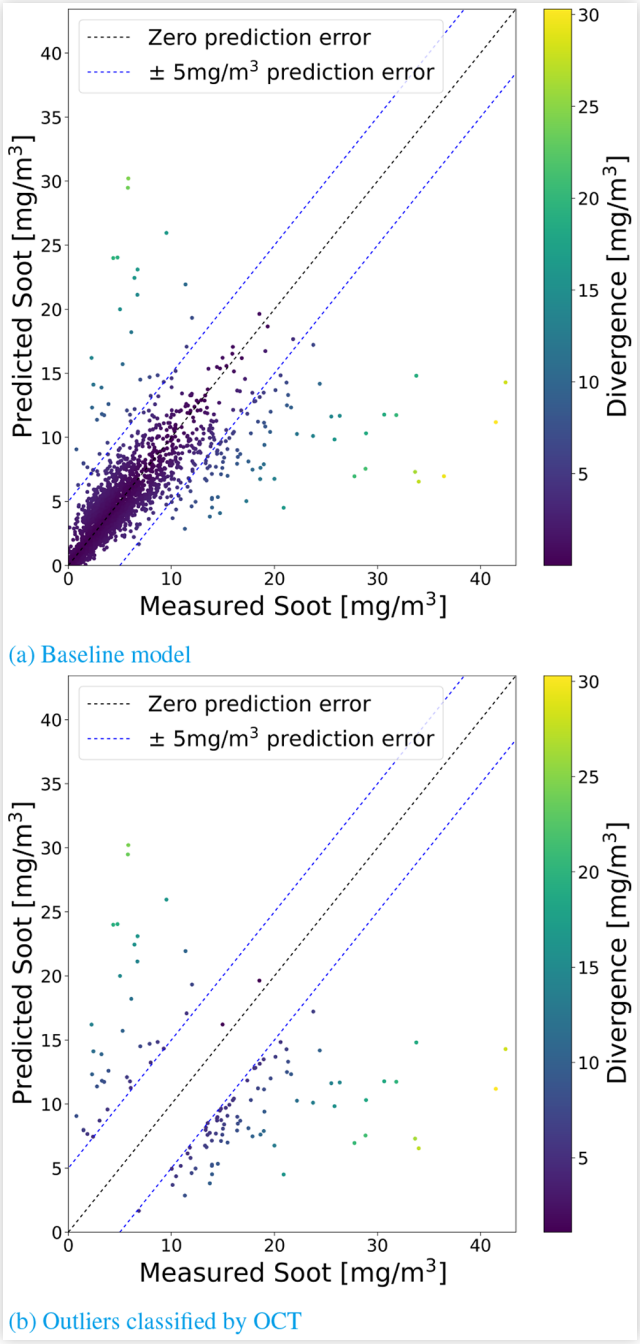

(a) Baseline model

(b) Outliers classified by OCT

FIGURE 6 Scatter plots of input and output points of the RFR model

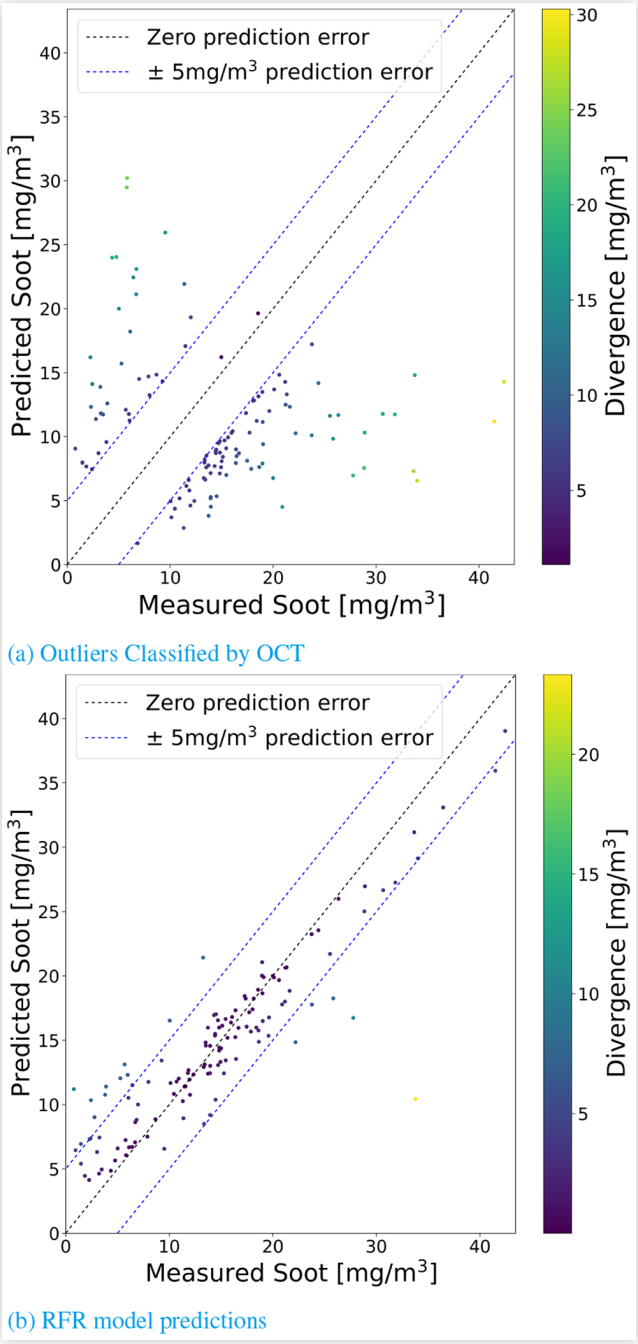

(a) Outliers Classified by OCT

(b) RFR model predictions

was trained on the original dataset with an 80%-20% train-test split for 20 iterations and the FI measures for each input feature were recorded. Figure 7 illustrates the mean FI values with their respective error bars. Feature $X5$ (engine-out soot mass with a 1-timestep lag) had the highest FI values and features $X2$, $X7$, and $X9$ had the lowest FI values. Based on the relative FI values, the extended list of input features was narrowed down to the 7 features that had the highest FI values. They are listed in Table 8.

The RFR model was trained on different values of the *maxDepth* constraint. The mean RMSE values were recorded for each value of tree depth and the trend is shown in Figure 8. The RFR model was then further trained on different values of the *nEstimators* constraint. The mean RMSE values were recorded for each value of the number of decision tree estimators and the trend is shown in Figure 9.

The scatter plots in Figure 6 illustrate the prediction performance of the RFR model. The input features of the OCT-classified-outliers plotted in Figure 6a are fed into the RFR as input and the predictions plotted in Figure 6b are the produced output.

FIGURE 7 Error Box plot of feature importance for Physics-based Random Forest Regressor

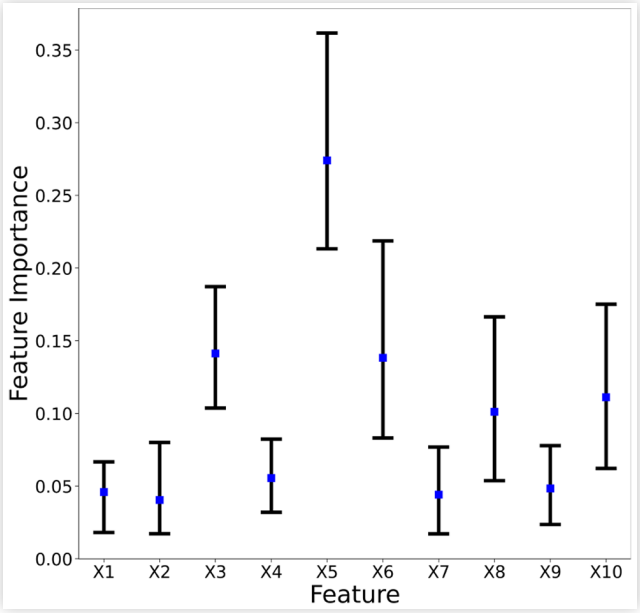

TABLE 8 Final input features for Physics-based Random Forest Regressor

Feature	Feature Symbol
m_{O_2}	X1
T_{adiab}	X3
m_{fg}	X4
$m_{s_{k-1}}$	X5
engSpd	X6
engSpdDelta	X8
fuelRateDelta	X10

FIGURE 8 RMSE trend with varying individual maximum tree depth for the RFR model

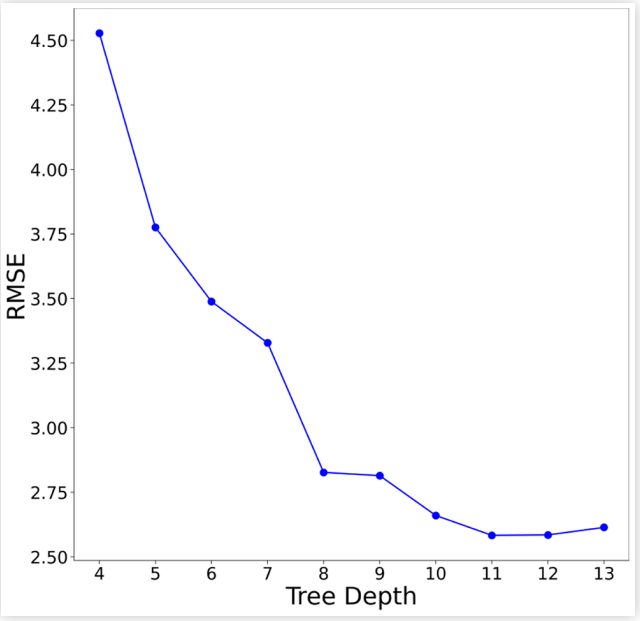

FIGURE 9 RMSE trend with varying number of estimators for the RFR model

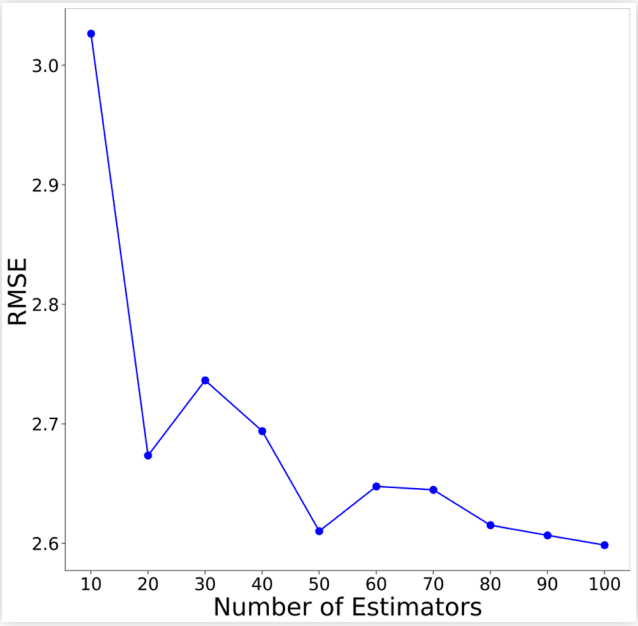

Complete Framework for Soot Mass Prediction and Analysis

To address the inability of the physics-based model to represent the soot-formation dynamics under transient engine operating conditions, a twin-model Physics-aware Classifier-Regressor (PaCR) Framework is proposed and summarized in Figure 10. The input to this framework is a set of engine features S at time t. The input is fed into the OCT that classifies the instance S as an outlier or an inlier. All inlier points are then fed into the Physics-based Regression Model. All outlier points are fed into the Random Forest Regression Model. The predictions from the respective regression models are then inferred and analyzed.

FIGURE 10 Physics-aware Classifier-Regressor (PaCR) Model Framework

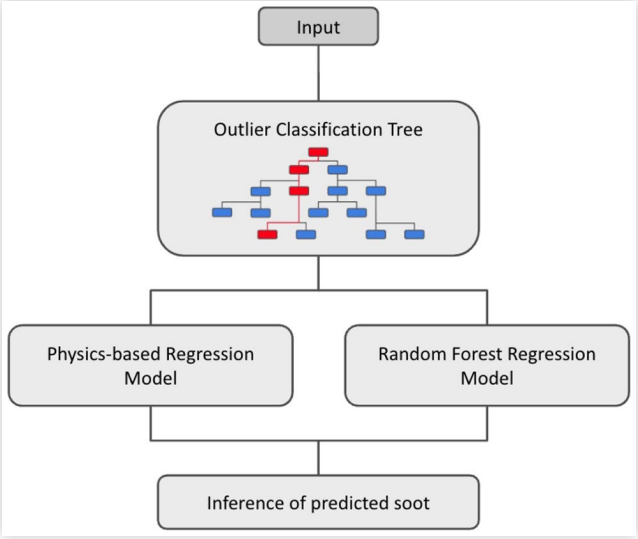

Results

Performance of the Twin-Model Framework

The values of the tunable parameters of the PaCR framework are set based on the analyses of the individual components of the framework and are listed in Table 9. The scatter plot illustrating the performance of the PaCR framework is shown in Figure 11. The performance metrics of the framework on the laboratory test dataset, along with other models are given in Table 10.

Comparison of the Proposed Framework with Non-Linear Regression

The proposed framework leverages the advantages of a random forest regressor to better predict engine-out soot mass in highly transient engine operating conditions when compared to using the baseline physics-based regression model as a standalone. Comparing the scatter plot of the baseline model (Figure 11a) with that of the PaCR framework (Figure 11c), conspicuous movement of initial outliers towards the zero-prediction-error line can be observed. Consequently, both the number of outlier points and the magnitude of the errors decrease with the PaCR framework.

Since in certain applications, the cumulative engine-out soot mass holds significance, the prediction error in the total soot mass can be observed and compared in Figure 12c. The cumulative soot mass plots generated using the baseline physics-based model (Figure 12a) and the PaCR framework (Figure 12c) can be assessed by comparing the d_1 values. The d_1 value is the absolute difference in the final values of the measured and predicted plots at the end of a fixed time period. The decrease in d_1 from 746.13 for the baseline model to 452.52 for the PaCR framework indicates that the proposed framework performs better. These changes are validated by the improved performance metrics (decreased RMSE and MAE, increased R^2) shown in Table 10.

Comparison of the Proposed Framework with a Deep Neural Network

The proposed framework was similarly compared to a fully connected deep neural network. The various architectures of

TABLE 9 Tuning parameters of the individual components of the twin-model framework

Component	Parameter	Value
OCT	*maxDepth*	8
	minSampleSplit	8
Random Forest Regressor	*maxDepth*	8
	nEstimators	20
	minSampleSplit	3

FIGURE 11 Scatter plots of engine-out soot mass prediction using the baseline physics-based non-linear regression, a physics-based DNN of size (256, 256, 256) and the PaCR framework

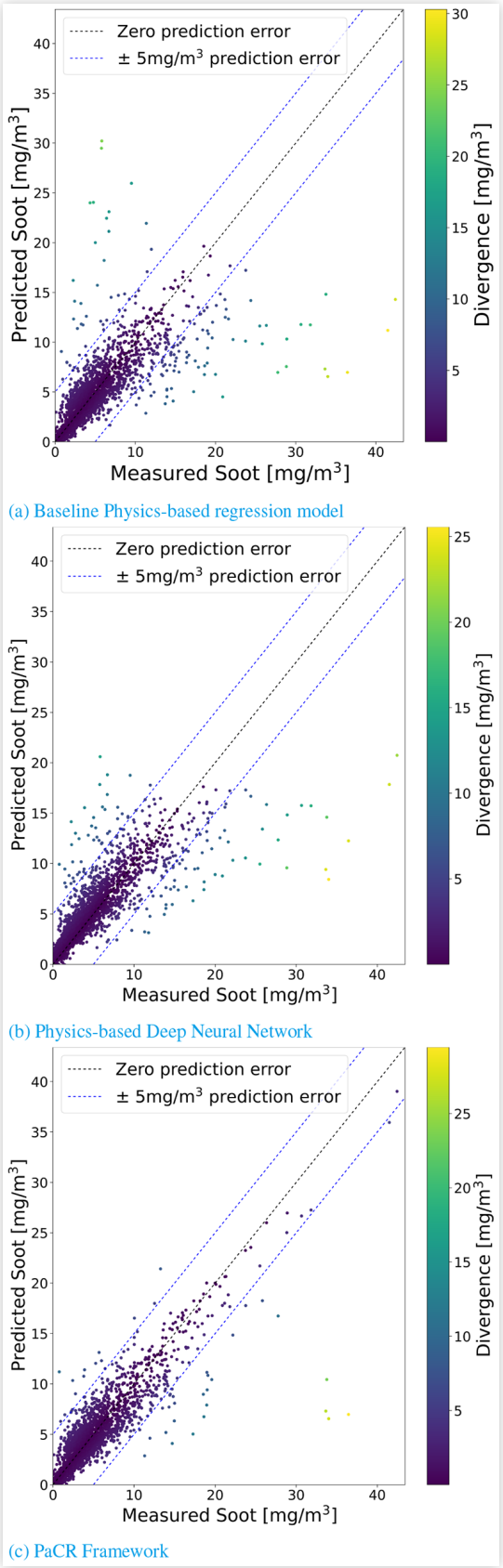

FIGURE 12 Engine-out cumulative soot mass prediction plots using the baseline physics-based non-linear regression, a physics-based DNN of size (256, 256, 256) and the PaCR framework

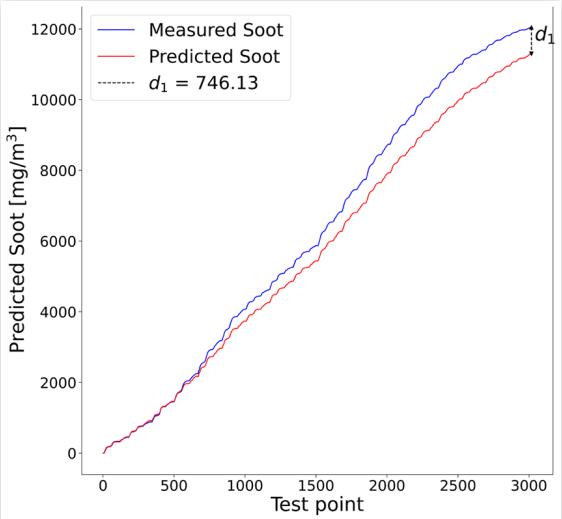

(a) Baseline Physics-based regression model

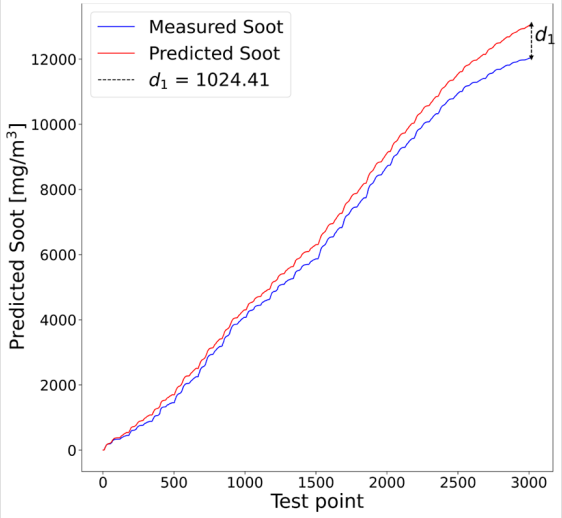

(b) Physics-based Deep Neural Network

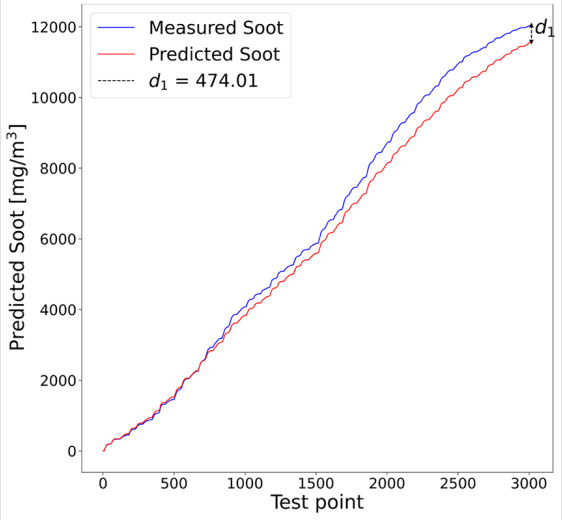

(c) PaCR Framework

TABLE 10 Performance Metrics of various models

Model	RMSE	MAE	R^2
Baseline Physics-based model	2.691	1.287	0.594
Physics-based DNN	2.183	1.284	0.701
Proposed Twin-Model Framework	1.882	1.048	0.801

FIGURE 13 Baseline model and RFR model predictions for input X_s

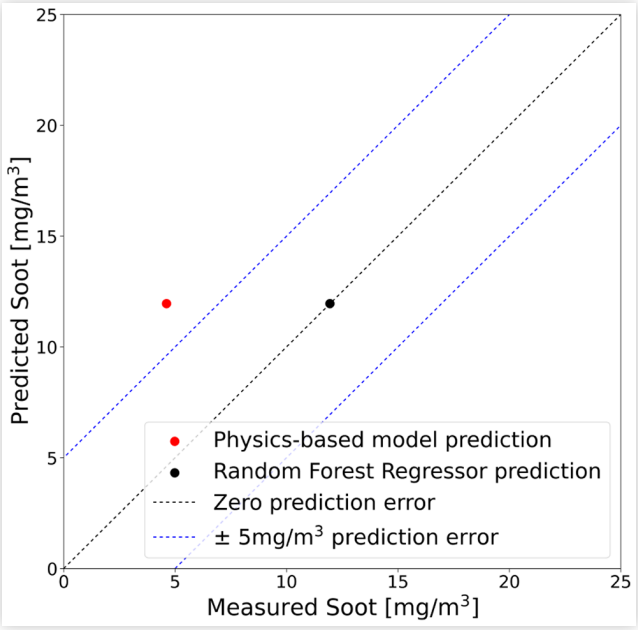

FIGURE 14 Explanation using SHAP values for input X*s*

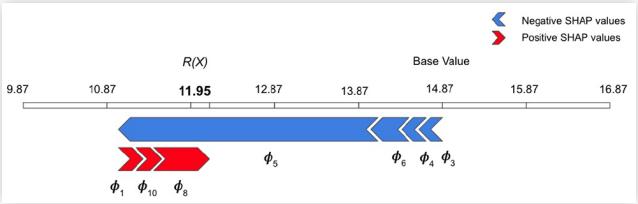

TABLE 11 Feature values and model predictions for sample X_s

Class	Parameter	Value
Input Feature	*X*1	8.51
	*X*3	1772.81
	*X*4	0.74
	*X*5	2.42
	*X*6	1311.68
	*X*8	10.53
	*X*10	0.26
Model Prediction	Physics-based model	4.61
	RFR model	11.95

TABLE 12 SHAP values for input X_s

SHAP measure	Value
ϕ_1	0.199
ϕ_3	-0.106
ϕ_4	-0.160
ϕ_5	-3.342
ϕ_6	-0.332
ϕ_8	0.612
ϕ_{10}	0.217

DNNs that were trained on the dataset along with their respective performance metrics are shown in Table 13 in the Appendix. The notation of the DNN size is of the format (n_1, n_2, …, n_m) where n_i represents the number of nodes in the i^{th} hidden layer and m represents the number of hidden layers. The DNN was designed to have either 2, 3, or 4 hidden layers, each containing either 64, 128, 256, or 512 nodes. Each hidden node was followed by a ReLU activation block and a normalization layer. The set of input features listed in Table 6 (same as the input feature set for the twin-model framework) was used for the DNN. The DNN was trained on 70% of the dataset using the Adam solver for a maximum of 200 iterations. The batch size for training was set to 200 samples. A termination criterion was set in place that ended the training process if the training loss fails to improve by 0.0001 over 10 iterations.

The training process for the DNNs shown in Table 13 stopped when the termination criterion was met. The loss convergence plots for the training and testing dataset for the different architectures are shown in Figure 17. It was observed that the loss values evaluated from the training set and the testing set converged for all the DNN models. Additionally, the loss plots for both sets exhibited similar trends and showed a high degree of alignment with each other.

For comparison, the DNN of size (256, 256, 256) was chosen because it had the highest R^2 error and the lowest RMSE among the tested models. Comparing the scatter plot of the chosen DNN (Figure 11b) with that of the PaCR framework (Figure 11c), it can be observed that the outlier points moved closer to the zero-prediction-error line. Similarly comparing the cumulative soot mass plot from the DNN model (Figure 12b) with that of the proposed framework (Figure 12a), the d_1 value decreases from 1024.41 (in the case of the DNN) to 452.52 (in the case of the twin-model framework). The decreased RMSE, decreased MAE, and the increased R^2 values (Table 10) as a result of using the PaCR framework instead of the physics-based DNN confirms the better prediction accuracy of the proposed framework.

Discussion

Prediction Inferences

The performance assessment of the PaCR framework along with the comparative analyses with the baseline physics-based model and a more complex, fully connected, deep neural network clearly show that the proposed framework is highly effective at predicting engine-out soot mass. The input feature variables for each component of the framework were carefully selected to emulate the highly complex kinetics of soot formation in GDI engines. The proposed framework presents a grey-box alternative to the DNN because the OCT and the Physics-based Regression Model are considered interpretable by design. They satisfy all three levels of transparency: simulatability (the ability of a model to be simulated or thought about strictly by a human), decomposability (the ability to explain each part of a model, i.e. inputs, parameters, and calculations), and algorithmic transparency (the ability of the user to understand the steps employed by the model in generating a specific output based on a specific input). However, random forest models are not interpretable by design [25]. They are often classified as black-box models but the predictions of such models can be partially explained using post-hoc explainability techniques like explanation by simplification and feature relevance techniques [25].

Discussion of the physical interpretation of the twin-model approach is also warranted. The results of this work show that the physics-based model is not sufficient to predict soot mass emissions during transient conditions. It is well known that transient conditions in GDI engines lead to fuel-surface interactions with the cylinder liner and piston, which are known to create soot-generating diffusion flames that have different soot formation mechanisms than normal premixed flame propagation. In a prior study with the same engine used in this work, it was shown that soot formation from pool fires was common with late fuel injection where fuel spray is more targeted at the cylinder top [26]. Other work illustrates that transient operation can lead to wall wetting with subsequent soot formation [27]. Therefore, using the outlier detection protocol developed in this framework to identify points where a different soot prediction model is implemented is considered a reasonable and explainable approach.

To explain the prediction instances of the Physics-based Random Forest Regressor in the proposed framework, we adapt the concept of SHAP (Shapley Additive Explanation) values [28] to the problem of soot mass prediction. SHAP values are a type of feature relevance measure that represents the change in the expected model prediction when the model is conditioned on a particular feature [28]. Explaining a prediction instance using SHAP values requires an *explainer* instance and the explanation consists of the following steps:

1. The explainer begins with a base value that represents the model prediction assuming no knowledge of any of the input features. This value is typically the expected value of the model predictions $E[R(X)]$, where $R(X)$ denotes the prediction by the random forest regressor for an input feature set X.
2. The SHAP values for each feature are calculated in a random sequence. If the SHAP value ϕ_1 for the first featureX_1 is calculated first, then ϕ_1 is the difference between $E[R(X)|X_1 = a_1]$ and $E[R(X)]$. Similarly, ϕ_2 for the feature X_2 is the difference between $E[R(X)|X_1 = a_1, X_2 = a_2]$ and $E[R(X)|X_1 = a_1]$. Consequently, the SHAP values move the prediction from the base value to the actual output of the model $R(X)$.

3. Since with complex models, the order of the features for which the SHAP values are calculated directly affects the final explanation and consequently, the explanation of the prediction, the above process is repeated for all possible combinations of the input features.

As an example to illustrate the prediction explanations of the Random Forest Regressor in the PaCR framework, a sample point X_s is taken from the laboratory test dataset. The relevant information about the sample point X_s for the explanation process is given in Table 11. The two prediction values, one from the baseline model and one from the RFR model, using X_s are plotted in Figure 13. The chosen sample X_s is an outlier as the distance between the physics-based model's prediction when given the input X_s and the zero-prediction-error line in Figure 13 satisfies the outlier classification criterion C_o in Equation 6. The *shap* python module introduced in [28] was used for illustrating the explanation of a prediction instance.

The relative magnitudes of the SHAP values of the individual input features are illustrated in Figure 14. The explainer begins with a base value of 14.87. This is equal to the mean value of the predictions of the RFR model. From the base value, the explainer shifts the prediction by each of the SHAP values ϕ_1 to ϕ_{10} to finally reach the actual output of the RFR model $R(X) = 11.95$. The SHAP values of each feature indicate the magnitude and direction of the influence that the feature had in moving the prediction from the base value to the actual prediction. The sign of the SHAP values only determines the direction in which the prediction moves from the base value. The SHAP values for the sample X_s are given in Table 12.

Future Work

Future improvements to the work presented in this paper include two avenues for exploration. First, the dataset used for the development of the proposed framework and its analyses is small and limited to laboratory experiments on one type of engine. In a continuation of this work, data collection from a different GDI engine is proposed and the PaCR framework will be validated on the new dataset with the aim of increasing its generalizability. Second, further refinement of the individual components of the PaCR framework will be pursued, with possible extension to the implementation of other data-driven models that are either interpretable by design or can be explained using post-hoc explainability techniques.

Conclusion

In this work, a novel, physics-aware twin-model machine learning framework is presented to accurately predict engine-out soot mass from measurable engine data. The input features for each of the components of the twin-model framework were carefully selected by a combination of DWC pattern detection and feature importance analyses repeated over randomly sampled batches of data. The proposed framework was observed to provide high predictive accuracies with the ability to be robust to outlier data points. Physical reasoning for the twin-model framework is that two separate soot formation mechanisms are at play in GDI engines precluding the use of a single physics-based approach. Prediction using the proposed framework provided, on average, 29% lower RMSE, 18% lower MAE, and 34% higher R^2 score, when compared to the baseline physics-based model. It also provided around 13% lower RMSE, 16% lower MAE, and 14% higher R^2 score, when compared to a physics-based deep neural network.

To fulfill the constraint of developing an interpretable emissions prediction framework, a post-hoc explainability technique involving SHAP values of the feature set was used to explain prediction instances of the Random Forest Regressor, since the RFR was the only component that was not interpretable by design. The high effectiveness of the proposed framework further strengthens the assumption that the underlying mechanism of soot formation in a GDI engine is a complex set of processes that varies with vehicle operating conditions.

References

1. Southerland V.A., Brauer M., Mohegh A., Hammer M.S., van Donkelaar A., Martin R.V., Apte J.S., and Anenberg S.C., "Global Urban Temporal Trends in Fine Particulate Matter (pm2·5) and Attributable Health Burdens: Estimates from Global Datasets," *The Lancet Planetary Health*, vol. 6, pp. e139-e146, 2 2022.
2. Thunis P., Pisoni E., Bessagnet B., Wilson J., Vignati E., Meij A.D., Mascherpa A., and E. C. J. R. Centre., Urban PM2.5 Atlas: Air Quality in European Cities: 2021 report.
3. Niranjan, R. and Thakur, A.K., "The Toxicological Mechanisms of Environmental Soot (black Carbon) and Carbon Black: Focus on Oxidative Stress and Inflammatory Pathways," *Frontiers in Immunology* 8 (2017): 6.
4. N. 1967-Janssen and W. R. Fur Europa, Health Effects of Black Carbon. World Health Organization, Regional Office for Europe, 2012.
5. Chen L., Liang Z., Zhang X., and Shuai S., "Characterizing Particulate Matter Emissions from GDI and PFI Vehicles under Transient and Cold Start Conditions," *Fuel*, vol. 189, pp. 131-140, 2 2017.
6. Piock, W., Hoffmann, G., Berndorfer, A., Salemi, P. et al., "Strategies Towards Meeting Future Particulate Matter Emission Requirements in Homogeneous Gasoline Direct Injection Engines," *SAE International Journal of Engines* 4 (2011). https://doi.org/10.4271/2011-01-1212.
7. Raza, M., Chen, L., Leach, F., and Ding, S., "A Review of Particulate Number (PN) Emissions from Gasoline Direct Injection (GDI) Engines and their Control Techniques," *Energies* 11 (6 2018): 1417.
8. Frenklach, M., "Reaction Mechanism of Soot Formation in Flames," *Physical Chemistry Chemical Physics* 4 (5 2002): 2028-2037.
9. Martyr, A.J. and Rogers, D.R., *Engine Exhaust Emissions* (Elsevier, 2021)
10. Zhao, F., Yang, W., and Yu, W., "A Progress Review of Practical Soot Modelling Development in Diesel Engine Combustion," *Journal of Traffic and Transportation Engineering (English Edition)* 7 (6 2020): 269-281.

11. Hiroyasu, H., Kadota, T., and Arai, M., "Development and Use of a Spray Combustion Modeling to Predict Diesel Engine Efficiency and Pollutant Emissions: Part 1 Combustion Modeling," *Bulletin of JSME* 26 (1983): 569-575.
12. Cheng, X., Chen, L., Yan, F., and Dong, S., "Study on Soot Formation Characteristics in the Diesel Combustion Process based on an Improved Detailed Soot Model," *Energy Conversion and Management* 75 (11 2013): 1-10.
13. Moss, J., "Modeling Soot Formation and Burnout in a High Temperature Laminar Diffusion Flame Burning under Oxygen-Enriched Conditions," *Combustion and Flame* 101 (6 1995): 491-500.
14. Tao, F., Golovitchev, V.I., and Chomiak, J., "A Phenomenological Model for the Prediction of Soot Formation in Diesel Spray Combustion," *Combustion and Flame* 136 (2 2004): 270-282.
15. Tao, F., Foster, D.E., and Reitz, R.D., "Characterization of Soot Particle Distribution in Conventional, Non-Premixed Di Diesel Flame Using a Multi-Step Phenomenological Soot Model," *Proceedings of the Combustion Institute* 31 (1 2007): 2991-2998.
16. Tao, F., Reitz, R.D., Foster, D.E., and Liu, Y., "Nine-Step Phenomenological Diesel Soot Model Validated over a Wide Range of Engine Conditions," *International Journal of Thermal Sciences* 48 (6 2009): 1223-1234.
17. Bidarvatan, M., Thakkar, V., Shahbakhti, M., Bahri, B. et al., "Grey-Box Modeling of HCCI Engines," *Applied Thermal Engineering* 70 (9 2014): 397-409.
18. Selvam H.P., Shekhar S., and Northrop W.F., "Prediction of no ¡sub¿x¡/sub¿ Emissions from Compression Ignition Engines Using Ensemble Learning-based Models with Physical Interpretability," 9 2021.
19. Shahpouri, S., Norouzi, A., Hayduk, C., Rezaei, R. et al., "Soot Emission Modeling of a Compression Ignition Engine Using Machine Learning," *IFAC-PapersOnLine* 54 (2021): 826-833.
20. Bock, N.R. and Northrop, W.F., "Influence of Fuel Properties on Gasoline Direct Injection Particulate Matter Emissions over First 200 s of World-Harmonized Light-Duty Test Procedure Using an Engine Dynamometer and Novel "Virtual Drivetrain" Software," *Journal of Energy Resources Technology* 143 (2021): 1-9.
21. Turns, S.R., *An Introduction to Combustion: Concepts and Applications*, 2nd ed. (McGraw-Hill series in mechanical engineering, Boston: WCB/McGraw-Hill, 2000)
22. Virtanen, P., Gommers, R., Oliphant, T.E., Haberland, M. et al., "Scipy 1.0: Fundamental Algorithms for Scientific Computing in Python," *Nature Methods* 17 (3 2020): 261-272.
23. Ali, R.Y., Gunturi, V.M.V., Kotz, A.J., Eftelioglu, E. et al., "Discovering Non-Compliant Window Co-Occurrence Patterns," *GeoInformatica* 21 (10 2017): 829-866.
24. Svetnik V., Liaw A., Tong C., Culberson J.C., Sheridan R.P., and Feuston B.P., "Random Forest: A Classification and Regression Tool for Compound Classification and QSAR Modeling," *Journal of Chemical Information and Computer Sciences*, vol. 43, pp. 1947-1958, Nov. 2003. Publisher: American Chemical Society.
25. Arrieta, A.B., Díaz-Rodríguez, N., Ser, J.D., Bennetot, A. et al., "Explainable Artificial Intelligence (xai): Concepts, Taxonomies, Opportunities and Challenges Toward Responsible AI," *Information Fusion* 58 (6 2020): 82-115.
26. Jeon, J., Bock, N., Kittelson, D.B., and Northrop, W.F., "Correlation of Nanoparticle Size Distribution Features to Spatiotemporal Flame Luminosity in Gasoline Direct Injection Engines," *International Journal of Engine Research* 21 (9 2020): 1107-1117.
27. Etikyala, S., Koopmans, L., and Dahlander, P., "Visualization of Soot Formation in Load Transients During GDI Engine Warm-Up," *International Journal of Engine Research* (12 2022): 146808742211411.
28. Lundberg S.M. and Lee S.-I., "A Unified Approach to Interpreting Model Predictions," in *Advances in Neural Information Processing Systems (I)*, Guyon, U.V. Luxburg, S. Bengio, H. Wallach, R. Fergus, S. Vishwanathan, and Garnett R., eds., vol. 30, Curran Associates, Inc., 2017.

Contact Information

Dr. William Northrop, Director, TE Murphy Engine Research Laboratory,
University of Minnesota-Twin Cities;
wnorthro@umn.edu
http:/merl.umn.edu
Ph: (612)-625-6854

Acknowledgments

This material is based upon work supported by the National Science Foundation under Grant No. 1901099. Data was collected for the framework with generous funding from the U.S. Department of Energy, Office of Energy Efficiency and Renewable Energy (EERE), under Award Number DE-EE0007217.

Definitions, Acronyms, Abbreviations

Acronyms

CO - Carbon Monoxide
DLS - Damped least-squares
DWC - Divergent Window Co-occurrence
FI - Feature Importance
GDI - Gasoline Direct Injection
GPF - Gasoline Particulate Filters
HC - Hydrocarbon
MAE - Mean absolute error
NO_x - Oxides of Nitrogen
OCT - Outlier Classification Tree
PaCR - Physics-aware Classifier-Regressor
PM - Particulate matter
R^2 - Coefficient of determination
RFR - Random forest regressor
RMSE - Root mean squared error
WLTP - Worldwide Harmonised Light Vehicles Test Procedure

Definitions

a, b, c, d,* and *q - Coefficients of physics-based model

A_f, A_c - constants

c_{pi} - temperature-dependent specific heat of species *i*

E_f, E_{sc} - the activation energies of soot formation and soot oxidation

LHV - Lower heating value of gasoline

m_s - mass of net soot

m_{fg} - mass of vaporized fuel

m_{sc} - mass of oxidized soot

m_{sf} - mass of formed soot

MW_{fuel} - Molecular weight of gasoline

p - cylinder pressure

T - cylinder temperature

T_{adiab} - Adiabatic flame temperature

T_c - chamber temperature at the end of compression stroke

X_{O_2} - mole fraction of oxygen during combustion

airRateDelta - Rate of change of air mass flow rate

airRate - air mass flow rate

brakeTorqueDelta - Rate of change of brake torque

brakeTorque - Brake Torque

engSpdDelta - Rate of change of engine speed

engSpd - Engine Speed

fuelRateDelta - Rate of change of fuel flow rate

fuelRate - Fuel flow rate

intakeP - Intake manifold pressure

intakeT - Intake manifold temperature

Appendix A

FIGURE 15 A sample OCT with tree depth = 4

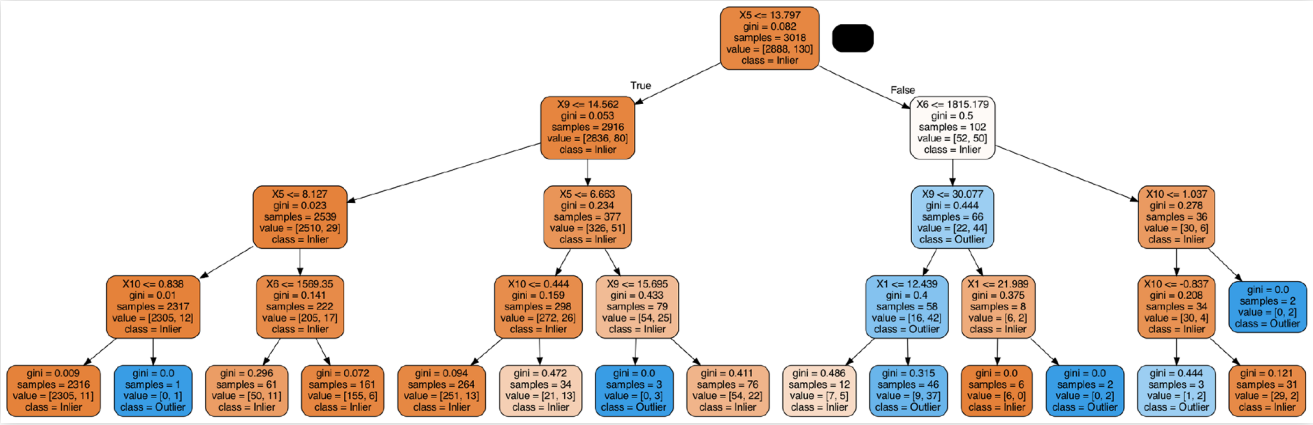

FIGURE 16 A sample decision tree from the Physics-based Random Forest Regressor with tree depth = 10

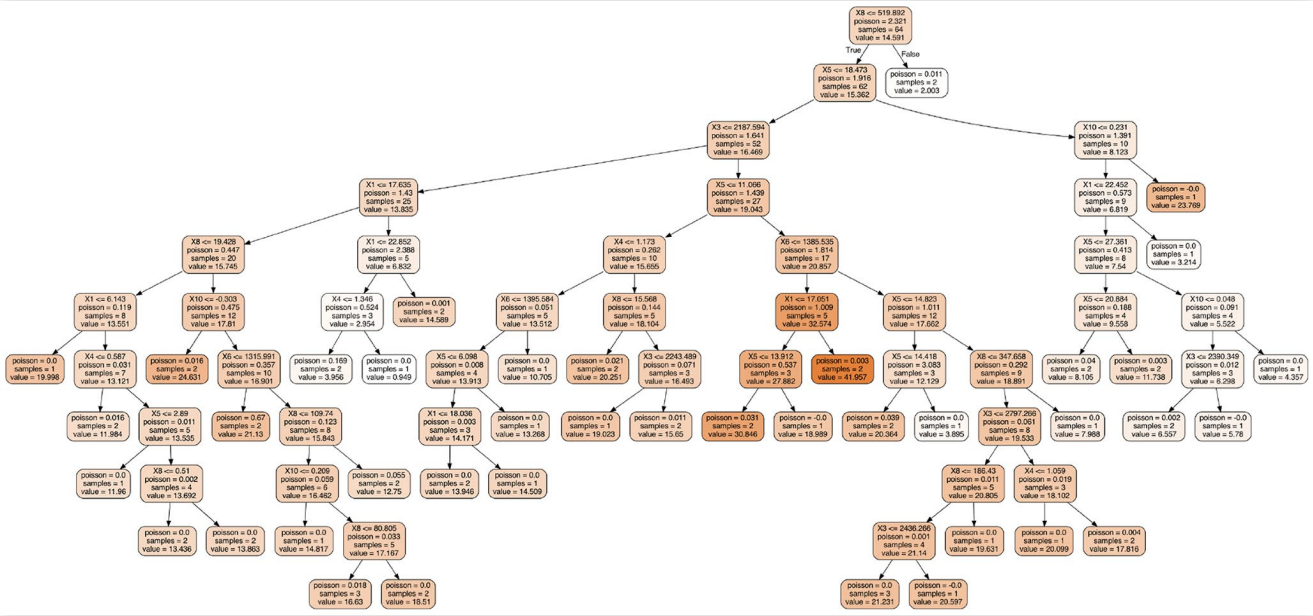

TABLE 13 Performance Metrics of deep neural networks with varying sizes. The notation of the DNN size is of the format $(n_1, n_2, ..., n_m)$ where n_i represents the number of nodes in the i^{th} hidden layer.

DNN size	RMSE	MAE	R^2
(128, 128)	3.578	2.892	0.221
(256, 256)	2.981	2.132	0.411
(512, 512)	2.547	1.524	0.633
(64, 64, 64)	2.808	1.812	0.512
(128, 128, 128)	2.289	1.188	0.667
(256, 256, 256)	2.183	1.284	0.701
(512, 512, 512)	2.588	1.325	0.647
(64, 64, 64, 64)	2.498	1.248	0.620
(128, 128, 128, 128)	2.330	1.233	0.644
(256, 256, 256, 256)	2.258	1.111	0.646

FIGURE 17 Loss Convergence for deep neural network of varying sizes

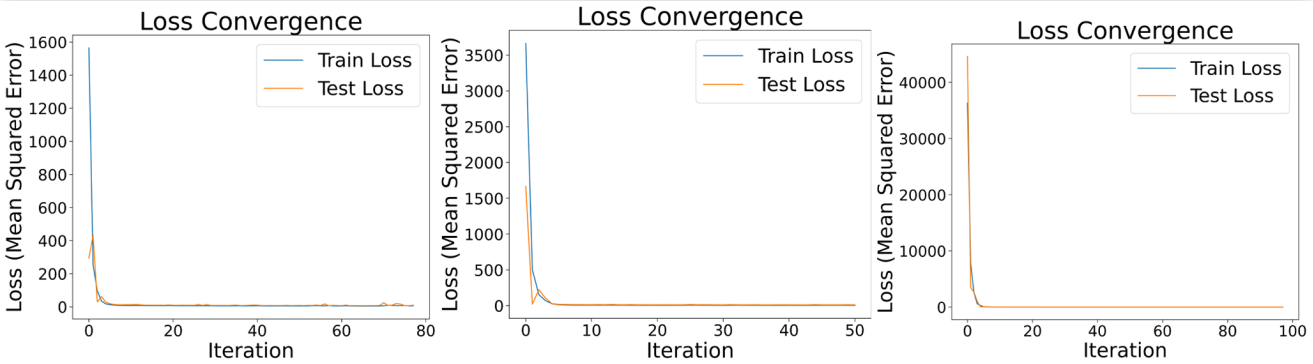

(a) Loss Convergence for deep neural network of size (128, 128)

(b) Loss Convergence for deep neural network of size (256, 256)

(c) Loss Convergence for deep neural network of size (512, 512)

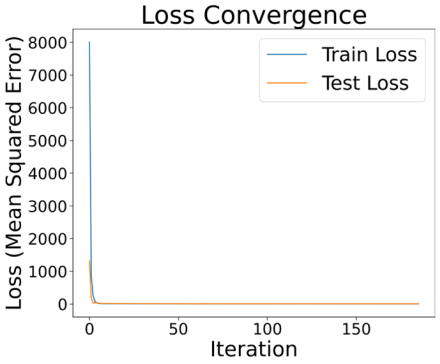

(d) Loss Convergence for deep neural network of size (64, 64, 64)

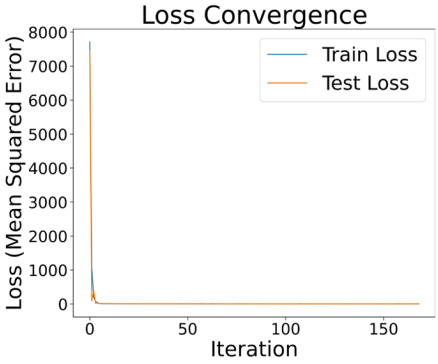

(e) Loss Convergence for deep neural network of size (128, 128, 128)

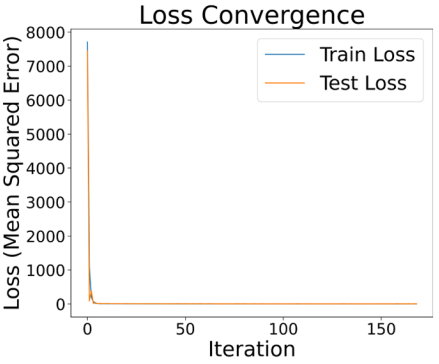

(f) Loss Convergence for deep neural network of size (256, 256, 256)

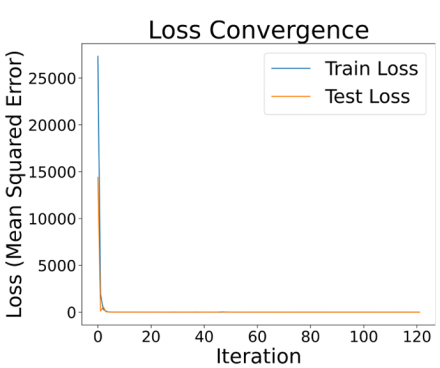

(g) Loss Convergence for deep neural network of size (512, 512, 512)

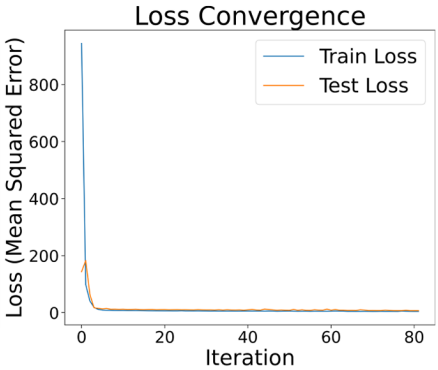

(h) Loss Convergence for deep neural network of size (128, 128, 128, 128)

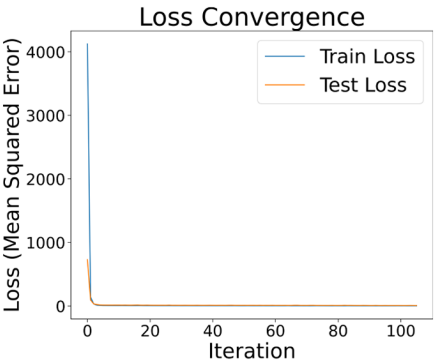

(i) Loss Convergence for deep neural network of size (256, 256, 256, 256)

ISSN 0148-7191